On the effect of Al on alumino-borosilicate glass chemical durability

Stephane Gin (stephane.gin@cea.fr)
CEA, DES, ISEC, DPME, University of Montpellier, Marcoule https://orcid.org/0000-0002-1950-9195
Kamalesh Damodaran
CEA
Jean-Marc Delaye
CEA Marcoule

Article

Keywords:

Posted Date: January 18th, 2023

DOI: https://doi.org/10.21203/rs.3.rs-2466755/v1

Additional Declarations: (Not answered)

Version of Record: A version of this preprint was published at npj Materials Degradation on May 30th, 2023. See the published version at https://doi.org/10.1038/s41529-023-00364-3.

Abstract

The chemical durability of borosilicate glass used to confine nuclear wastes non-linearly depends on a slight variation of their composition. Here, we focus on Al, a major oxide of these materials. Both matrix dissolution and long term-rates are investigated through experiments conducted at 90°C and pH 9. We demonstrate that low Al content glasses dissolve initially faster than glasses with higher Al content, but they form a gel that reorganized faster and eventually becomes more passivating. These results can be tied to recent findings at the molecular level showing that Al impacts the activation energy of Si–O bond breaking. The implications for the geological disposal of high-level waste glass of these findings are discussed.

Introduction

The chemical durability of borosilicate glasses has been the subject of many studies ever since certain countries chose this material as a containment matrix for long-lived radioactive waste [1–3]. However, nuclear glasses are very complex materials (> 20 oxides), and studying the reaction mechanisms between the glass and water demands working with simplified model materials. Therefore, since 2013, the scientific community has used a six-oxide borosilicate glass, called ISG glass, as the reference to establish a robust knowledge base concerning the dissolution mechanisms and kinetics of nuclear glasses [1,4,5]. In a silica-rich solution, ISG glass dissolution is slowed down by several orders of magnitude compared to the initial dissolution rate because of an affinity reduction effect on the silicate network dissolution reaction, and by forming a passivating gel layer between the glass and the solution [6,7]. The glass dissolution rate which results from these processes is called the residual rate. The physical and chemical processes at microscopic or even molecular scale that limits the residual rate remain to be established [6]. Many studies have focussed on the formation and maturation of the passivating gel layers formed on nuclear glasses (for more details, see the following review articles by Frankel et al.[4], Gin et al.[5], and Thorpe et al.[8]). Diffusion properties of hydrous species in these gels depend on the composition of the glass and the solution (Si concentration, pH), temperature, maturation time, and to a certain extent, on the glass structure. Besides, short and medium structural order within the glass depends on the cooling rate and the irradiation conditions [9,10]. The question of whether or not there is a link between the glass structure, the gel properties, and the residual rate still remains open [11]. Finding an answer would enable a better understanding of the passivating layer formation mechanism and thereby open the way to develop reliable kinetic models to predict these materials' long-term behavior.

This study focuses on 6 Na-aluminoborosilicate glasses with Al_2O_3 content ranging from 0 to 6 mol%. Their initial dissolution rates are measured at 90°C pH 9 to determine the rate of matrix dissolution in the absence of passivating layer. The rate drop related to solution feedback and passivation layer effects is studied with a six-month static test in deionized water. Finally, a third experiment is conducted by selecting a glass sample from low Al content glass and a high Al content glass to investigate how the gel becomes passivating. This experiment involves a ^{29}Si spiked solution and solid-state characterization with ToF-SIMS. Overall these experiments demonstrate that Al dramatically affects matrix dissolution and gel reorganization, with a huge impact on the glass dissolution rate.

Results And Discussion

Initial dissolution rate

Figure 1 shows the evolution of the normalized mass loss of Si arising from the experiments conducted at 90°C, pH 9, low glass-surface-area-to-solution-volume (SA/V), and short duration (6 hours). Initial dissolution rates, r_0, which correspond to the fastest dissolution rate for a given temperature and pH, are obtained by linear regression of the normalized mass loss. Note that, in this study, *NL*(Si) are calculated according to Eq. 1, using the BET surface area although a previous study[12] concluded that for powder the actual reactive surface area is closer to the geometric surface than the BET one. We made

this choice to allow comparison with the long-term data for which the same normalization was applied. The ratio between the BET surface area and the geometric one is close to 2 for all glasses (Table 1). Thus, this choice would not affect the comparisons among the glasses of this series. The values of r_0 are given in Fig. 1. First, it can be noted that glass SBNA0 has a value of r_0 in agreement with already published data for this glass: glass called CJ1 in Gin et al. (2012)[13] in which a value of 4.5 $g.m^{-2}.d^{-1}$ was reported; Glass called SBN14/18 in Gin et al. (2020)[14] in which a value of 12 $g.m^{-2}.d^{-1}$ was reported. This last value was obtained with the geometric surface area, a value generally 2 to 3 times lower than the BET surface area of the powder.

Regarding our series, globally, low Al content glasses (up to 1 mol% Al_2O_3) dissolve at a rate close to 5 $g.m^{-2}.d^{-1}$, whereas glasses with higher Al content dissolve around five times slower, i.e., at a rate close to 1 $g.m^{-2}.d^{-1}$. From a previous study[12], it was determined that the uncertainty on r_0 is ± 30%. Therefore the difference between the two groups of glasses is significant. It is in agreement with previous work showing that when Si is replaced by Al in ISG, glass durability in dilute conditions is highly improved up to 12 mol% of Al_2O_3 [15]. Authors believe two possible mechanisms by which Al increases the durability of glass. (i) Al reduces the Na co-ordination with non-bridging oxygen (weak), and increases the Na co-ordination with Al (strong). (ii) Second mechanism proposes that Al is increasing the network connectivity of glass, which reduces the diffusion of water.

In this study, when we compare the initial dissolution rate of SBNA0 with SBNA1, we observed that r_0(SBNA1) > r_0(SBNA0), due to an excess of Na content in SBNA1. This is in agreement with the first mechanism proposed, according to which, we expect the addition of Al to strengthen Na and increase the durability of glass. But this reason is not sufficient. A recent atomistic simulation study using molecular dynamics (MD) demonstrated that Al being second neighbor to Si increases the activation energy for dissociating the bonds around Si [16]. Authors also suggest that, when Al strengthens Si and increases the network connectivity of glass, diffusion of water might be reduced due to rate limiting step for dissociating four- and three-fold coordinated Si in the presence of Al around it. Accordingly, our study observed r_0 decreases with increasing concentration of Al content in glass. This is clearly the case when comparing SBNA1bis and SBNA3.5 which have the same amount of Si and B. This study along with previous MD simulation results strongly support the idea that Al strengthening Si could be an important reason for increased durability of glass in the r_0 regime.

180-day alteration experiments

Static experiments have been conducted at high S/V, 90°C, and pH 9 for six months. As reactors were placed in a second container filled with water, evaporation of the solution was negligible. First, it can be noted that, in all the experiments, the pH remains stable over time and close to the target value (9.0 ± 0.2). Figure 2 shows the time dependence of the concentration of Si, *C(*Si*)*. In all cases, *C(*Si*)* readily increases and eventually achieves a plateau characterized by stable, or slightly increasing concentrations, which can be considered as the saturation of the solution with respect to the gel. The height of the plateau broadly varies depending on the glass composition. The three glasses with the lowest Al content (SBNA0, SBNA1, and SBNA1bis) have the highest *C(*Si*)*, between 400 and 500 $mg.L^{-1}$, whereas the glasses with increasing concentration of Al display a decreasing *C(*Si*)* at saturation. Note also that the results for SBNA1 and its replicate (SBNA1_R) are similar.

As silica in basic solution can dissociate, form oligomers or complex with sodium, the Jchess geochemical code[17] was employed to calculate the activity of silica in the 6 solutions at 3 durations. Results are plotted in Fig. 3 in two ways: First, as saturation index with respect to amorphous silica for 4 of the 6 glasses are displayed for readability (Fig. 3a) and second as the mean value against the percentage of Al_2O_3 in the glass (Fig. 3b). These calculations indicate that all the solutions remain undersaturated with respect to amorphous silica, but the degree of undersaturation increases with the content of Al in the glass. More precisely, the value of the plateau achieved for each glass diminishes linearly with the concentration of alumina in the glass (Fig. 3b). This result suggests that the presence of Al in the glass efficiently controls

the release of Si into the solution. Let us discuss the reason. The concentration of Si in solution results from both dissolution and condensation reactions. At equilibrium, the rate of the two opposite reactions are equal. The trend depicted in Fig. 3b is in agreement with recent atomistic simulations showing that Al as second neighbor in aluminosilicate glass strengthens the Si (i.e. enhances the activation energy for dissociating Si–O bonds and decreases the activitation energy for the Si-O bond reformation), so that the rate of Si dissolution is reduced, at least for glass with low Al content[16]. Further calculations performed with Potential Mean Force and ReaxFF confirmed that the activation energies for bond dissociation and bond reformation are respectively larger and lower in aluminosilicate glass than pure silicate glass [18]. This means that aluminosilicate gels require less energy to form that pure silica gel. This result is in agreement with a lower solubility of aluminosilicate gel.

In borosilicate glass alteration study, B and Na are usually selected to monitor the glass dissolution rate, especially when backward reactions of condensation or precipitation control the net release of other glass constituents into the solution[5,6]. To be valid, this choice requests that B and Na released from the glass are not retained in any solid (gel, secondary phases), so that the measurement of their concentration in the solution can be used to calculate the amount of reacted glass. In most cases, this assumption is assumed to be valid but is not verified. Recently, we demonstrated that i) in some circumstances, B can be retained in the gel layer and that this retention could impact the rate of glass alteration[6], ii) B diffusion coefficients in gels are low ($\sim 10^{-20}$ $m^2.s^{-1}$ in gel of ISG formed at pH 9)[19], iii) B retention and diffusion in gels strongly depend on the pH and the presence of Ca[19].

Following this classical assumption that B can be used as a tracer, Equivalent thickness of the altered glass was calculated from B concentrations and plotted against the square root of time (Fig. 4). Note that Equivalent thickness of altered glass are given for all the elements in SI. Globally B and Na give the same trend, although values for Na are lower than that for B in high Al content glasses, suggesting that Na could be retained in the gel to charge compensate four-fold cocordinated Al atoms. Regarding B behavior, it appears that the three glasses with a low Al content dissolve rapidly during the first days and eventually achieve a very slow dissolution rate. Conversely, the three glasses with a higher Al content dissolve slowly at the beginning, but their dissolution rate diminishes extremely slowly. Moreover, for the two glasses with the highest Al content (SBNA4 and SBNA6), a linear release with square root of time is noticed, followed by a slower regime after approximately 80 days. For glass SBNA3.5, a continuous decrease of B release rate is observed. Finally, the duplicated tests provide the same results.

Overall, this series of glasses shows that the amount of Al in the glass strongly influences the dissolution rate of glass. Therefore, the most durable glasses in Si-saturated conditions are those with a low concentration of Al, contrary to what is expected from the initial dissolution regime. To go further, we calculated the ratio between the initial dissolution rate, r_0, and the final rate obtained by linear regression between 110 days and 180 days. This ratio allows us to estimate the magnitude of the rate drop due to the formation of the gel layer. It is of the order of 4000 for SBNA0, > 40000 for glasses SBNA1 and SBNA1bis, 1000 for glass SBNA3.1, 200 for glass SBNA4, and 150 for glass SBNA6. Although these figures are valid only at a specific duration as the rate of some glasses are still evolving even after 6 months, they can still highlight the differences between glasses within the series. It thus clearly appears that glasses with low Al content form more passivating gels. The next experiment will try to better understand the reasons why.

One month experiment

The one-month experiment was conducted with two glasses, one from the low Al content glasses, SBNA1, and the other from the high Al content glass, SBNA4. For this experiments, we used only glass coupons and performed ToF-SIMS depth profiling after the reaction. The leaching solution was pre-saturated with $^{29}SiO_2$, and the $pH^{90°C}$ was adjusted to 9.0 with LiOH. These conditions were chosen to ensure a rapid saturation of the solution with respect to the gel. Because of the low SA/V ratio selected for this experiment, it would have taken long time to reach the saturation state if the onset solution was

free of Si. At the end of the experiment, the glass coupon was immersed for 24 h in ^{18}O labeled water. This tracing solution was free of Si but this second stage was conducted at room temperature to minimize further gel and glass alteration. The equivalent thickness of altered glass was calculated from B and Na concentrations (Fig. 5). Data show that SBNA1 glass corrodes incongruently (Na is released faster than B) and the dissolution rate dramatically drops beyond 10 days. Conversely, SBNA4 glass corrodes congruently and its dissolution rate remains almost constant over the experiment's duration. Note that Al concentrations were below detection limit. Compared to previous experiments conducted with glass powder, some differences are noticed:

- For SBNA1, B and Na are not released at the same rate, whereas the dissolution was congruent in the long-term experiment. ToF-SIMS characterization will help understand the reason why B is released slower than Na.
- For SBNA4, B and Na are released at the same rate whereas some Na was retained in the gel in the long-term experiment.

Despite these differences, the altered glass' thickness at the end of 1-month experiment are similar to that determined with powder at the same duration. For the two studied glasses the differences noted above can arise from the fact that the gel can form since the beginning of the reaction in the short term experiment due to the addition of silica in the starting solution unlike the experiment with powder which started in a solution free of Si.

ToF-SIMS depth profiles are presented in Fig. 6. First, it can be noticed that unlike SBNA4 glass, B is partly retained in the gel formed on SBNA1. The retention of B in SBNA1 gel is the reason why the dissolution of this glass is incongruent. Moreover, the amount of Na retained in the two gels is very small, meaning that this element can be considered as a good dissolution tracer. As the transition between glass and gel is marked by the depletion front of B and Na, it is remarkable to see that the depletion fronts for B and Na are located at the same depth for each glass. This strongly suggests that Na release is limited by B dissolution, as it was already observed for ISG.

Despite the presence of 250 ppm of ^{29}Si in the solution, both gels keep the isotopic signature of the natural abundance (Fig. 6c, d). This result is a strong indication that the two glasses turn into gel by in situ hydrolysis/condensation reactions instead of dissolution/reprecipitation. As a reminder, is was shown in a previous study that an Al-free borosilicate glass similar to SBNA0 forms a gel by dissolution/reprecipitation[20]. Thus, a small amount of Al seems to be sufficient to switch to another mechanism of gel formation. Third, $^{18}O/^{16}O$ ratio recorded in the two gels are different (Fig. 6e, Fig. 6f). The profile increases towards the glass in gel SBNA1 whereas it is flat and much lower in gel SBNA4. The blue line indicates the value of $^{18}O/^{16}O$ which should be achieved if all the porosity left by the release of B and Na is filled with ^{18}O labelled water. The way to calculate this curve is explained in a former paper[19]. For SBNA1 the porosity decreases toward the glass because of the retention of B in the gel. A counterintuitive result is that the $^{18}O/^{16}O$ ratio increases with decreasing porosity.

There are two possible explanations to account for this result, either water molecules from the bulk solution fill the open pores and the result highlights the location of the open pores only, or these water molecules preferentially exchange with the gel skeleton (OH groups, bridging oxygen (O_{br})) and do not fill all the pores. The first hypothesis suggests that closed pores mostly occupy the outer part of the gel, whereas the second hypothesis suggests that the most reactive sites are located deeper in the gel, up to the reaction front. Looking at SBNA4 gel, first hypothesis seems unlikely because the glass dissolution rate does not decrease, which means that the gel is not or poorly passivating, whereas the fraction of filled pores is extremely small compared to the total porosity. The only possibility to keep this option open would be that pore water has evaporated during the analysis (due to the low pressure in the analysis chamber). One cannot totally rule out this option but the analysis has been run in cryogenic mode, and validation has been made that this mode preserves most of the pore water during the analysis[21]. Therefore it can be thought that some pores even open are not filled with labelled water. This hypothesis is supported by recent classical MD simulations with MGFF dissociative potentials[22]. In this study the authors introduced water in dry aluminosilicate gels containing pores[23]. The simulations showed that water molecules

diffuse inside the gel skeleton and let some empty space within the pores. When these empty spaces are refilled with more water, the same phenomenon takes place, showing that the driving force led water molecule to enter the gel skeleton. This phenomenon is conformed in another simulation study performed on amorphous silica nanotubes [24]. Thus, the signal recorded from ^{18}O tracing experiment would be more representative of the reactivity of the gel skeleton instead of the pore distribution. Following this idea, the correlation between B retention and ^{18}O enrichment suggests that O preferentially exchange with O binding B atoms. This hypothesis is in agreement with previous results showing a sharp increase of $^{18}O/^{16}O$ ratio in the inner region of ISG gels where B is trapped[11,25]. This is also confirmed by the conclusion obtained on ISG showing that, in silica saturated conditions, glass dissolution is controlled by the breaking of B-O-Si linkages[6].

The case of SBNA1 is of great interest because its alteration ceases – or at least becomes extremely slow – during the course of the experiment and some B is detected in the gel. Recent work has shown that the retention of B in the gel retroacts on the continuation of the glass alteration reaction, not through water diffusion as it was suspected before[26] but more likely through further hydrolysis of B–O–Si linkages and diffusion of B_{aq} [19]. In that particular case, it can be proposed that the fast reorganization of the gel, highly permitted by the low concentration of Al, favors B retention in the inner region of the gel, which in turn dramatically reduce the rate at which glass continues to corrode. In that sense, gel reorganization appears to be a key step in glass protection by amorphous surface layer.

Borosilicate glass are designed to contain large amounts of radionuclides (18 wt% of waste in R7T7 glass produced in France [27], up to 35 wt% of waste loading in some UK MW glasses [28]) while guaranteeing high resistance against irradiation and water [29,30]. According to our results, one can wonder if adding more Al into nuclear waste containment glasses could improve glass performance in geological disposal conditions. It is demonstrated that Al improves glass durability in the first kinetic regime (initial dissolution rate), whereas an opposite effect is observed in the residual rate regime as Al in glass delays the formation of the passivating gel. Adressing this question requires to know what will be the geochemical conditions near the glass in the actual geological disposal conditions. There is no unique and trivial answer to this question, because it depends both on the site, the nature of nearfield materials, and of course the time period considered as conditions in the disposal cells will evolve. Indeed, materials in the vicinity of the glass could be reactive and thus could impact glass durability [31]. For instance, it is known that Fe present in the primary canister and the overpack is soluble in anoxic and reducing environments, and could react with Si from the glass to form iron silicate minerals at the expense of the gel [32–37]. Furthermore, hostrock can release in porewater elements such as Mg and Ca, or organic acids that can react with the glass [38–41]. Often, reactions taking place between exogenous and glass elements decrease glass durability because many secondary and non passivating phases can form at the expense of the gel in the pH-T conditions of the disposal (typically $6 < pH < 9$, $25°C < T < 90°C$) [42]. A safe approach would then be to formulate glasses with the lowest possible initial dissolution rate. This will ensure the lowest reactivity in the presence of deleterious element supplied by the environment. Another interest is that glasses with high Al content display lower concentrations of Si at saturation, which means that more stable gels can form. These behaviors are more advantageous than forming quickly a passivating gel. Indeed, the dissolution rate of the high Al content glasses tested in this study still diminish with time, meaning that the gel formed on these materials become passivating. The time scale that seems important in our laboratory studies is negligible on the storage time scale. The trends above discussed have been confirmed by an experimental comparison between ISG – a deeply studied peralkaline glass with 3.8 mol% Al_2O_3 – and a peraluminous glass containing 15 mol% Al_2O_3. Interestingly, the latter is significantly less susceptible to clayey groundwater and highly alkaline solutions [43]. The initial dissolution rate of this peraluminous glass is 2.5 times lower than that of ISG. The difference is significant but not huge because of the non-linear response of the glass upon composition variation [44]. There is more work to do to define optimized glass compositions. The current study suggests that increasing Al content in peralkaline glasses or switching to peraluminous glasses would be two interesting options for the future.

Methods

Glass preparation

Six Na-aluminoborosilicate glasses were prepared by melting oxide powders to eventually obtain a 200g-bar of each composition. Nominal compositions of the six glasses are given in Table 1. They are designed as SBNAx, where S stands for Si, B for B, N for Na, A for Al, and x the mol% of Al_2O_3 in the glass. For the 6 glasses the following procedure was applied. The mixture of powder was introduced in a Pt-Rh crucible, then heated in a furnace at 1450 K for 3 hours and 20 minutes. The molten glass was poured on the steel slab, then crushed after cooling and remelted at 1450°C to ensure a good homogeneity. The resulting molten glass was poured in a graphite mold and annealed for 1 hr at 550°C to anneal the glass. Glass composition was analyzed both by SEM-EDX (ZEISS MERLIN at CEA Marcoule, operating at 30 kV) and ICP-OES (FILAB France) after dissolution in acids. Both analytical techniques confirmed that actual composition match the nominal composition within analytical uncertainties (± 5%).

From the bars, small coupons with dimensions of 20 x 20 x 1 mm^3 were cut with a diamond saw. The 6 faces of each coupon were polished up to diamond paste of 1µm leading to a RMS < 5 nm. Crushed glass of 100–125 µm and 40–100 µm size fraction was also prepared by the classical procedure of crushing, sieving and ultrasonic cleaning in ethanol and acetone to remove fine particles. The specific surface area of the 40–100 µm powder was measured by Brunauer, Emmett and Teller (BET) method using Kr gas (uncertainty ± 5%).

Table 1 – Solution data sets. Concentrations measured by ICP-OES and ICP-MS, normalized mass losses and equivalent thicknesses of B.

	SiO_2	B_2O_3	Na_2O	Al_2O_3	Density ($g.cm^3$)	S_{geo} 100-125 µm ($cm^2.g^{-1}$)	S_{BET} 100-125 µm ($cm^2.g^{-1}$)	S_{geo} 40-100 µm ($cm^2.g^{-1}$)	S_{BET} 40-100 µm ($cm^2.g^{-1}$)
SBNA0	67.8	18	14.2	0	2.42	220	405	354	690
SBNA1	63	18.7	17.3	1	2.46	217	355	348	645
SBNA1bis	60.5	20.1	18.4	1	2.46	217	415	348	720
SBNA3.5	60.5	20.1	15.9	3.5	2.40	222	415	357	715
SBNA4	64.9	17.3	13.7	4.1	2.39	223	435	359	720
SBNA6	66.8	15.9	11.3	6	2.36	226	455	363	780

Table 1: Nominal compositions (mol%) of the six glasses designed to investigate the influence of Al on aluminoborosilicate glass. Density is calculated from Fluegel's model[45]. Geometric surface area and BET surface area of the two powders used in this study.

Initial dissolution rate measurement

Initial dissolution rate of the 6 glasses was measured at 90°C, $pH^{90°C}$ 9 in static mode with glass powder. More details are given in a previous paper (ref Gin V0 npj). Briefly, a small mass of 100–125 µm powder is put in perfluoroalkoxy (PFA) vessel containing 400 mL of the leaching solution. The pH of the solution was adjusted with LiOH 1M. Magnetic stirring insures that glass particles did not lie at the bottom of the reactor. The 6 tests are conducted in parallel, using an oven regulated at 90 ± 2°C. Solution is regularly sampled during the 6 hours of the experiment. It is then acidified with diluted nitric acid and analyzed by inductively coupled plasma-optical emission spectrometry (ICP-OES, FiLAB France).

From the elemental concentrations, normalized mass losses were calculated:

$$NL(i)_t = NL(i)_{t-1} + \frac{(C(i)_t - C(i)_{t-1}) \bullet V_t}{S \bullet x_i}$$

1

Where $C(i)_t$ is the concentration of element *i* in solution at the time *t*, V_t the volume of solution at time *t*, *S* the glass surface area determined from the BET specific surface area multiplied by the mass of glass, and x_i the mass fraction of the element *i* in the glass. *NL(i)* is expressed in $g.m^{-2}$. The equivalent thickness, which give the thickness of the glass that has been dissolved, based on the concentration of element *i* in solution, was calculated as follows:

$$ETh(i) = \frac{NL(i)}{\rho}$$

2

Where ρ is the density of the glass (Table 1).

Initial dissolution rate r_0 ($g.m^{-2}.d^{-1}$) is calculated in the linear regime from:

$$r_0 = \frac{d(NL(i))}{dt}$$

3

As r_0 refers to matrix dissolution, it is calculated from the release of Si. However, in this regime, glass dissolution is generally congruent, which means that the release rate of all glass cations is similar.

Concentrations, *NL(i)*, *Eth(i)*, and r_0 are given with 5%, 10%, and 30% uncertainty, respectively (Fournier 2016).

Long term experiments

Experiments were performed with the 6 SBNA glass powders. Experiments were conducted in 60 ml PFA vessels without magnetic stirring. Glass powder of mass ranging between 3.2092 to 3.8791 g were added to 50 mL of 18.2 MΩ.cm water whose $pH^{90°C}$ was fixed at 9.0 ± 0.1 with 10^{-2} M LiCl solution, so that the initial glass-surface-area-to-solution-volume (SA/V) was 50 cm^{-1}. High SA/V ratio was chosen to quickly allow the solution to saturate with silica. To limit evaporation, the reactors were held in an over-pack container, also made of PFA and containing a few mL of deionized water. At each sampling duration, the reactor was dried, weighed and opened. Approximately 0.5 ml was taken with a syringe, filtered with a cutoff of 0.2 µm and diluted with 2 ml of 0.5 N ultrapure HNO_3 solution. Samples were collected every 7 days during first month and then every 15 days for the next 5 months. Collected samples were analyzed with Inductively coupled plasma-optical emission spectrometry (ICP-OES, FiLAB France). Concentrations of Si, B, Na, and Al are given with an uncertainty of ± 5%.

Normalized mass loss, equivalent thickness, and rate are calculated using formulas 1–3. In this case, as Si concentrations achieved quickly a plateau corresponding to a saturation state, B and Na are used as tracer for glass alteration.

Static, 1-month leaching experiments

Experiments were conducted as follow. $^{29}SiO_2$ (Cortecnet, 99.69% of ^{29}Si) was dissolved 12.2 MΩ.cm water whose $pH^{90°C}$ was fixed at 9.0 ± 0.1 with 10^{-2} M LiCl solution to obtain 280 $mg.L^{-1}$ of ^{29}Si. 14 mL of this solution was introduced in a 20 mL PFA vessel with a polished glass coupon placed on a Teflon basket. 0.5 mL of solution was sampled every 7 days and diluted with 2 ml of ultrapure HNO_3 solution. These samples were analyzed with ICP-OES (Filab France) to measure the

concentration of Si, B, Na and Al in the solutions. At the end of the experiment the glass coupon was recovered, quickly rinsed with ultrapure water and incubated in tracing solution containing 99% of $H_2{}^{18}O$ for 24 hours at room temperature. ToF-SIMS depth profiling in both positive and negative modes was performed to investigate the depth wise ratio of $^{29}Si/^{28}Si$ and $^{18}O/^{16}O$ in the alteration layer. ToF-SIMS analysis was carried out in Tescan Analytics, Fuveau, France using ToF-SIMS 5 spectrometer (Iontof – Münster, Germany), with following conditions for positive mode: primary beam of $Bi_1{}^+$, 25 keV, I 0.2 pA with analyzed area of 50 x 50 μm^2 and sputter beam of 1 keV, 300 nA of Cs^+ with abrasion area of 200 x 200 μm^2. Similarly, ToF-SIMS conditions for negative mode were: Primary beam of $Bi_3{}^{++}$, 25 keV, 0.1 pA with analyzed area of 50 x 50 μm^2 and sputter beam of 2 keV, 94 nA of Cs^+ with abrasion area of 200 x 200 μm^2.

Declarations

DATA AVAILABILITY

The data that support the findings of this study are available from the corresponding authors on reasonable request.

ACKNOLEDGEMENTS

This study was supported as part of the center for Performance and Design of Nuclear Waste Forms and Containers, U.S. Department of Energy (DOE) [Award #DESC0016584].

AUTHORS CONTRIBUTION

S.G. supervised the study and wrote the paper. K.D. ran the experiments. All the authors participated to the scientific discussion and contributed to the editing of the manuscript under its present form.

COMPETING INTEREST

The authors declare no competing interests.

References

1. Gin, S. *et al.* An international initiative on long-term behavior of high-level nuclear waste glass. *Mater. Today* **16**, 243-248, doi:10.1016/j.mattod.2013.06.008 (2013).
2. Grambow, B. Nuclear waste glasses - How durable? *Elements* **2**, 357-364, doi:10.2113/gselements.2.6.357 (2006).
3. Ojovan, M. I., Lee, W. E. & Kalmykov, S. N. *An Introduction to Nuclear Waste Immobilisation*. 3rd edition edn, (Elsevier, 2019).
4. Frankel, G. S. *et al.* Recent Advances in Corrosion Science Applicable To Disposal of High-Level Nuclear Waste. *Chemical Reviews*, doi:10.1021/acs.chemrev.0c00990 (2021).
5. Gin, S., Delaye, J.-M., Angeli, F. & Schuller, S. Aqueous alteration of silicate glass: state of knowledge and perspectives. *npj Materials Degradation* **5**, 42, doi:10.1038/s41529-021-00190-5 (2021).
6. Gin, S. *et al.* Insights into the mechanisms controlling the residual corrosion rate of borosilicate glasses. *NPJ MATERIALS DEGRADATION* **4**, doi:10.1038/s41529-020-00145-2 (2020).
7. Neeway, J., Abdelouas, A., Grambow, B. & Schumacher, S. Dissolution mechanism of the SON68 reference nuclear waste glass: New data in dynamic system in silica saturation conditions. *Journal of Nuclear Materials* **415**, 31-37, doi:10.1016/j.jnucmat.2011.05.027 (2011).
8. Thorpe, C. L. *et al.* Forty years of durability assessment of nuclear waste glass by standard methods. *Npj Materials Degradation* **5**, doi:10.1038/s41529-021-00210-4 (2021).
9. Angeli, F. *et al.* Effect of thermally induced structural disorder on the chemical durability of International Simple Glass. *npj Materials Degradation* **2**, 31, doi:10.1038/s41529-018-0052-3 (2018).

10. Mir, A. H. & Peuget, S. Using external ion irradiations for simulating self-irradiation damage in nuclear waste glasses: State of the art, recommendations and, prospects. *Journal of Nuclear Materials* **539**, 30, doi:10.1016/j.jnucmat.2020.152246 (2020).
11. Tribet, M. *et al.* New Insights about the Importance of the Alteration Layer/Glass Interface. *Journal of Physical Chemistry C* **124**, 10032-10044, doi:10.1021/acs.jpcc.0c02121 (2020).
12. Fournier, M. *et al.* Glass dissolution rate measurement and calculation revisited. *Journal of Nuclear Materials* **476**, 140-154, doi:10.1016/j.jnucmat.2016.04.028 (2016).
13. Gin, S., Beaudoux, X., Angeli, F., Jegou, C. & Godon, N. Effect of composition on the short-term and long-term dissolution rates of ten borosilicate glasses of increasing complexity from 3 to 30 oxides. *J. Non-Cryst. Solids* **358**, 2559-2570, doi:10.1016/j.jnoncrysol.2012.05.024 (2012).
14. Gin, S. *et al.* Can a simple topological-constraints-based model predict the initial dissolution rate of borosilicate and aluminosilicate glasses? *Npj Materials Degradation* **4**, 10, doi:10.1038/s41529-020-0111-4 (2020).
15. Reiser, J. T. *et al.* Effects of Al:Si and (Al plus Na):Si ratios on the static corrosion of sodium-boroaluminosilicate glasses. *Int. J. Appl. Glass Sci.* **13**, 94-111, doi:10.1111/ijag.16109 (2022).
16. Damodaran, K., Delaye, J. M., Kalinichev, A. G. & Gin, S. Deciphering the non-linear impact of Al on chemical durability of silicate glass. *Acta Mater.* **225**, 14, doi:10.1016/j.actamat.2021.117478 (2022).
17. van der Lee, J., De Windt, L., Lagneau, V. & Goblet, P. Module-oriented modeling of reactive transport with HYTEC. *Comput. Geosci.* **29**, 265-275, doi:10.1016/s0098-3004(03)00004-9 (2003).
18. Damodaran, K. *Insights into the mechanisms controlling the dissolution of alumino-borosilicate glass and development of a new Monte Carlo model* PhD thesis, Montpellier, (2022).
19. Damodaran, K., Gin, S., De Montgolfier, J. V., Jegou, C. & Delaye, J. M. Behavior of B in passivating gels formed on International Simple Glass in acid and basic pH. *J. Non-Cryst. Solids* **598**, 9, doi:10.1016/j.jnoncrysol.2022.121938 (2022).
20. Gin, S. *et al.* A General Mechanism for Gel Layer Formation on Borosilicate Glass under Aqueous Corrosion. *Journal of Physical Chemistry C* **124**, 5132-5144, doi:10.1021/acs.jpcc.9b10491 (2020).
21. Collin, M. *et al.* ToF-SIMS depth profiling of altered glass. *npj Materials Degradation* **3**, 14, doi:10.1038/s41529-019-0076-3 (2019).
22. Taron, M. *Simulation à l'échelle nanoscopique du transport réactif : application à la dissolution des verres nucléaires* PhD thesis, Montpellier, (2022).
23. Taron, M., Delaye, J. M. & Gin, S. A classical molecular dynamics simulation method for the formation of "dry" gels from boro-aluminosilicate glass structures. *J. Non-Cryst. Solids* **553**, 11, doi:10.1016/j.jnoncrysol.2020.120513 (2021).
24. Daub, C. D., Cann, N. M., Bratko, D. & Luzar, A. Electrokinetic flow of an aqueous electrolyte in amorphous silica nanotubes. *Phys. Chem. Chem. Phys.* **20**, 27838-27848, doi:10.1039/c8cp03791d (2018).
25. Gin, S. *et al.* Origin and consequences of silicate glass passivation by surface layers. *Nature Communications* **6**, 8, doi:10.1038/ncomms7360 (2015).
26. Gin, S. *et al.* Dynamics of self-reorganization explains passivation of silicate glasses. *Nature Communications* **9**, 9, doi:10.1038/s41467-018-04511-2 (2018).
27. Vernaz, E. & Brueziere, J. in *2nd International Summer School on Nuclear Glass Wasteform - Structure, Properties and Long-Term Behavior (SumGLASS).* 3-9 (Elsevier Science Bv).
28. Fisher, A. J., Harrison, M. T., Hyatt, N. C., Hand, R. J. & Corkhill, C. L. The dissolution of simulant UK Ca/Zn-modified nuclear waste glass: the effect of increased waste loading. *MRS Adv.* **6**, 95-102, doi:10.1557/s43580-021-00025-0 (2021).
29. Donald, I. W. *Waste Immobilization in Glass and Ceramic Based Hosts: Radioactive, Toxic and Hazardous Wastes*. (Wiley, 2010).

30. Ojovan, M. I. & Lee, W. E. Glassy Wasteforms for Nuclear Waste Immobilization. *Metall. Mater. Trans. A-Phys. Metall. Mater. Sci.* **42A**, 837-851, doi:10.1007/s11661-010-0525-7 (2011).
31. Frankel, G. S. *et al.* Recent Advances in Corrosion Science Applicable To Disposal of High-Level Nuclear Waste. *Chemical Reviews* **121**, 12327-12383, doi:10.1021/acs.chemrev.0c00990 (2021).
32. Michelin, A. *et al.* Effect of iron metal and siderite on the durability of simulated archeological glassy material. *Corrosion Sci.* **76**, 403-414, doi:10.1016/j.corsci.2013.07.014 (2013).
33. Dillmann, P., Gin, S., Neff, D., Gentaz, L. & Rebiscoul, D. Effect of natural and synthetic iron corrosion products on silicate glass alteration processes. *Geochim. Cosmochim. Acta* **172**, 287-305, doi:10.1016/j.gca.2015.09.033 (2016).
34. Guo, X. L. *et al.* Near-field corrosion interactions between glass and corrosion resistant alloys. *Npj Materials Degradation* **4**, 15, doi:10.1038/s41529-020-0114-1 (2020).
35. Guo, X. L., Gin, S. & Frankel, G. S. Review of corrosion interactions between different materials relevant to disposal of high-level nuclear waste. *Npj Materials Degradation* **4**, 16, doi:10.1038/s41529-020-00140-7 (2020).
36. Guo, X. L. *et al.* Self-accelerated corrosion of nuclear waste forms at material interfaces. *Nat. Mater.* **19**, 310-+, doi:10.1038/s41563-019-0579-x (2020).
37. Schlegel, M. L. *et al.* Alteration of nuclear glass in contact with iron and claystone at 90 degrees C under anoxic conditions: Characterization of the alteration products after two years of interaction. *Appl. Geochem.* **70**, 27-42, doi:10.1016/j.apgeochem.2016.04.009 (2016).
38. Mann, C. *et al.* Influence of young cement water on the corrosion of the International Simple Glass. *Npj Materials Degradation* **3**, 9, doi:10.1038/s41529-018-0059-9 (2019).
39. Fisher, A. J. *et al.* Short communication: The dissolution of UK simulant vitrified high-level-waste in groundwater solutions. *Journal of Nuclear Materials* **538**, 7, doi:10.1016/j.jnucmat.2020.152245 (2020).
40. Gin, S., Godon, N., Mestre, J. P., Vernaz, E. Y. & Beaufort, D. EXPERIMENTAL INVESTIGATION OF AQUEOUS CORROSION OF R7T7 NUCLEAR GLASS AT 90-DEGREES-C IN THE PRESENCE OF ORGANIC-SPECIES. *Appl. Geochem.* **9**, 255-269, doi:10.1016/0883-2927(94)90036-1 (1994).
41. Jollivet, P. *et al.* Effect of clayey groundwater on the dissolution rate of the simulated nuclear waste glass SON68. *Journal of Nuclear Materials* **420**, 508-518, doi:10.1016/j.jnucmat.2011.10.026 (2012).
42. Jantzen, C. M., Trivelpiece, C. L., Crawford, C. L., Pareizs, J. M. & Pickett, J. B. Accelerated Leach Testing of Glass (ALTGLASS): II. Mineralization of hydrogels by leachate strong bases. *Int. J. Appl. Glass Sci.* **8**, 84-96, doi:10.1111/ijag.12264 (2017).
43. Piovesan, V. *et al.* Chemical durability of peraluminous glasses for nuclear waste conditioning. *Npj Materials Degradation* **2**, 10, doi:10.1038/s41529-018-0028-3 (2018).
44. Vienna, J. D., Ryan, J. V., Gin, S. & Inagaki, Y. Current Understanding and Remaining Challenges in Modeling Long-Term Degradation of Borosilicate Nuclear Waste Glasses. *Int. J. Appl. Glass Sci.* **4**, 283-294, doi:10.1111/ijag.12050 (2013).
45. Fluegel, A. Global model for calculating room-temperature glass density from the composition. *J. Am. Ceram. Soc.* **90**, 2622-2625, doi:10.1111/j.1551-2916.2007.01751.x (2007).

Figures

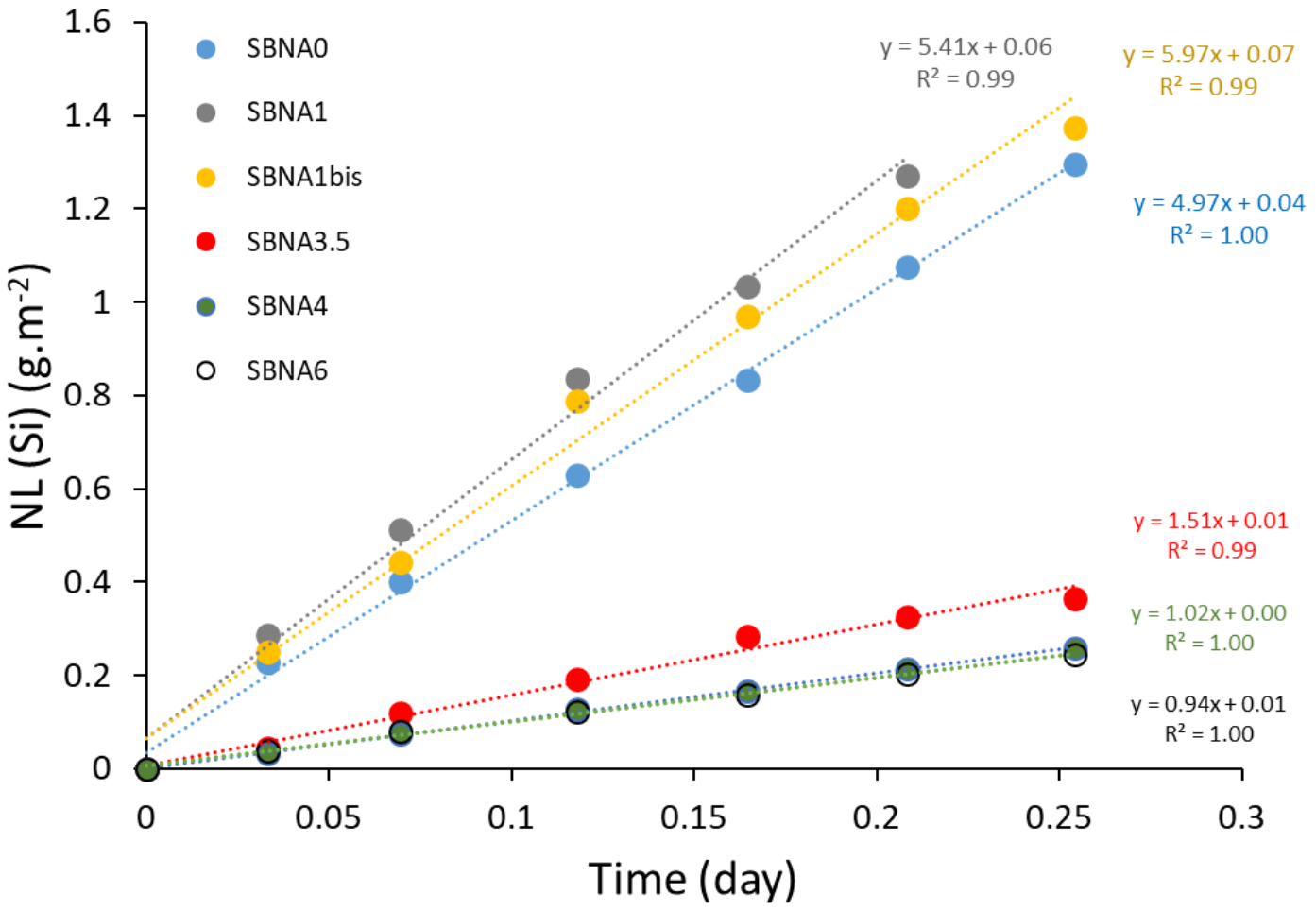

Figure 1

Initial dissolution rate of the 6 glasses measured at 90°C pH 9. Normalized mass loss for Si against time. The slope obtained by linear regression provides the initial dissolution rate, r_0.

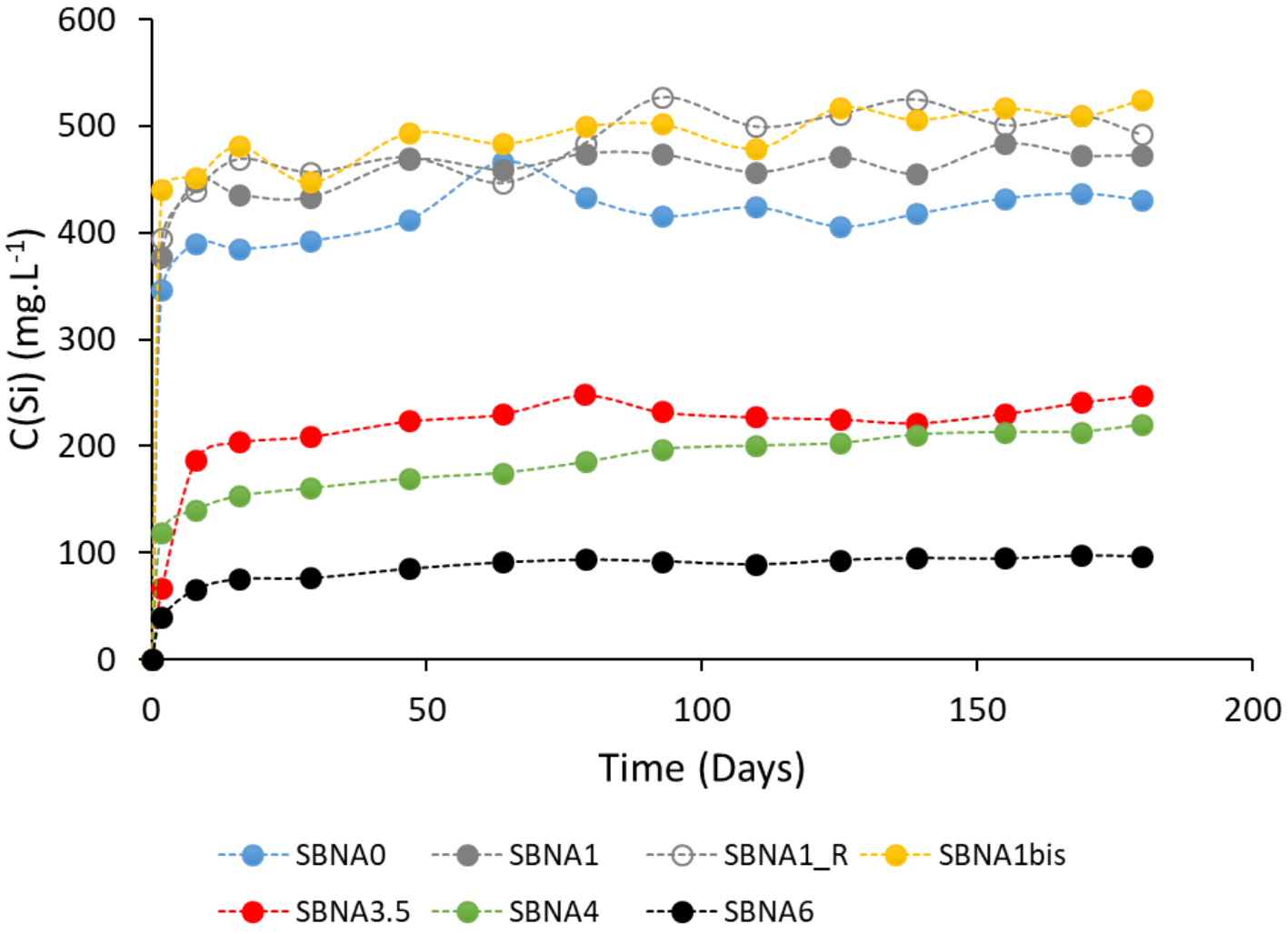

Figure 2

Concentration of Si from SBNA series of glasses. Uncertainty is ±5%. SBNA1_R is repeat of SBNA1 to verify the consistency of the dissolution experiments.

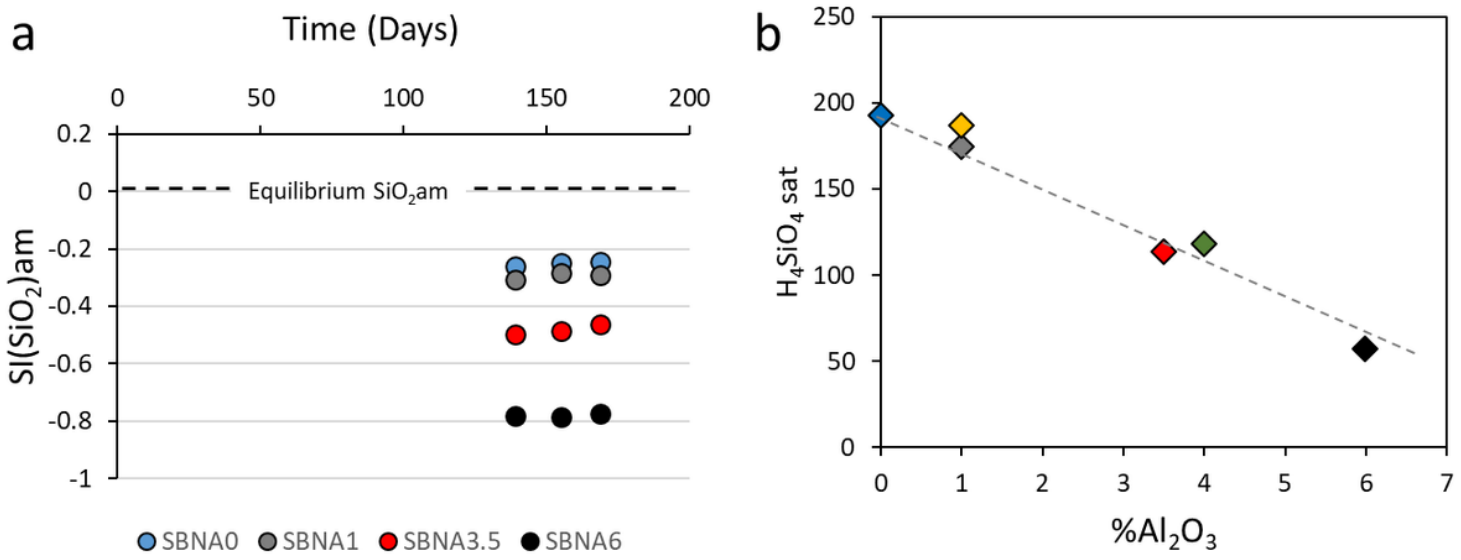

Figure 3

Activity of silica in the long-term experiments. **a**, Saturation index of the solutions with respect to amorphous silica. **b**, Correlation between the mean activity of silica in the solution vs concentration of Al_2O_3 in SBNA series of glasses. Linear regression of the correlation are displayed with dotted line. The same color code is used for the different experiments.

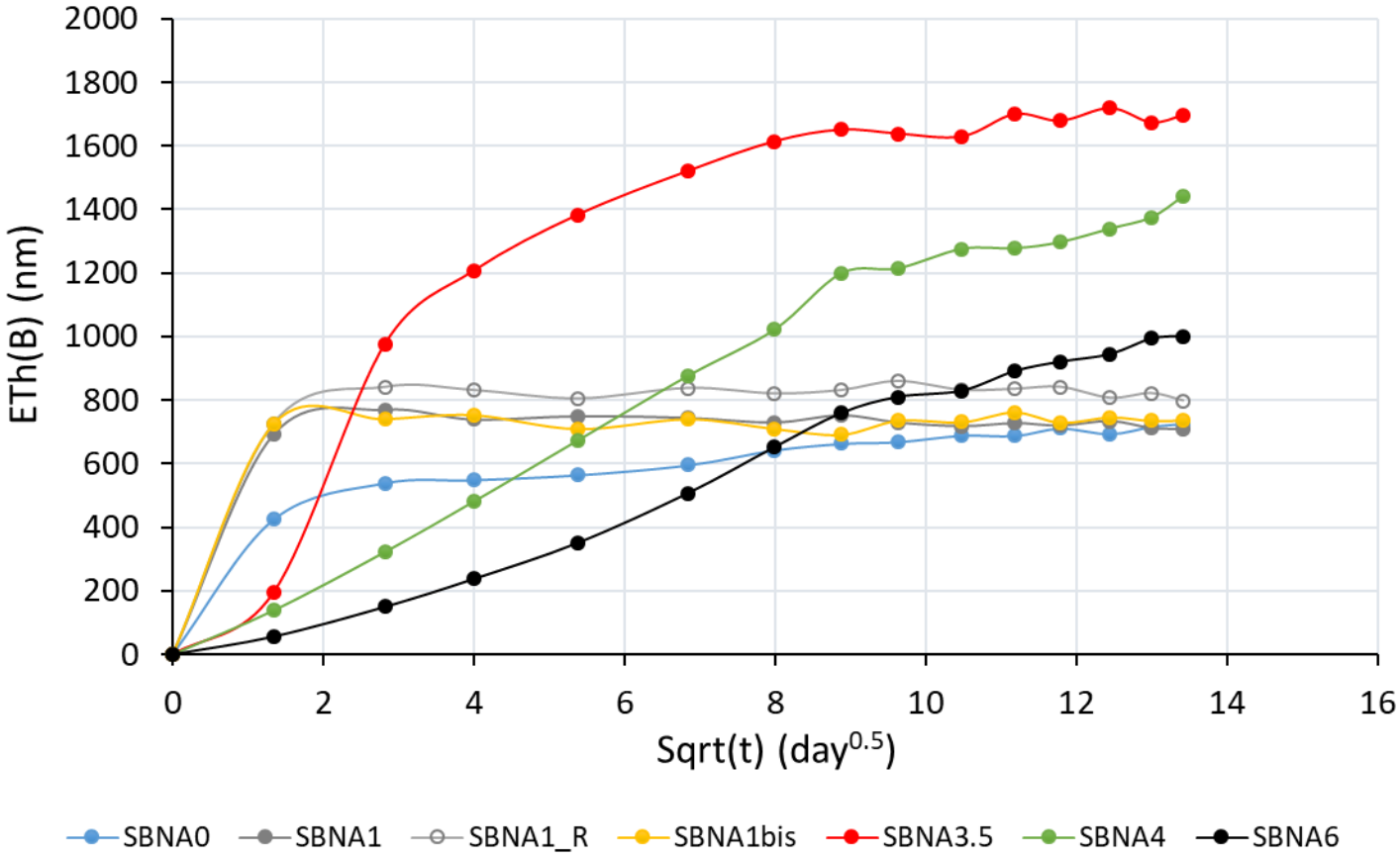

Figure 4

Long term dissolution of B from SBNA series of glasses recorded with respect to the square root of time. Color scheme for each glass are indicated appropriately. SBNA1_R is repeat of SBNA1 to verify the consistency of dissolution experiments.

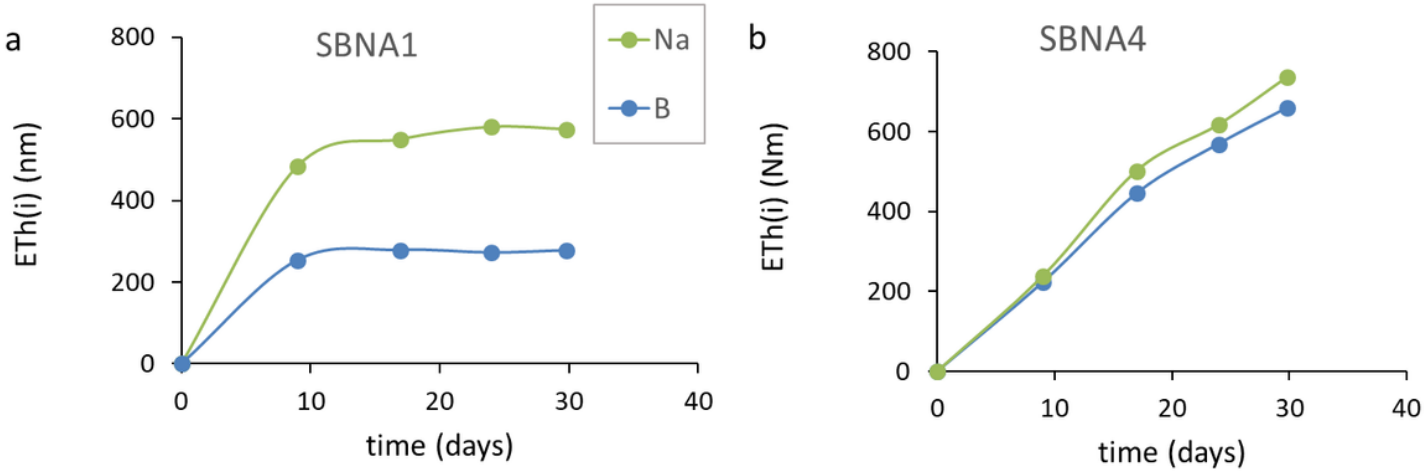

Figure 5

Solution data from the 1-month experiment. **a**, Equivalent thickness of B and Na for SBNA1 glass. **b**, Equivalent thickness of B and Na for SBNA4 glass.

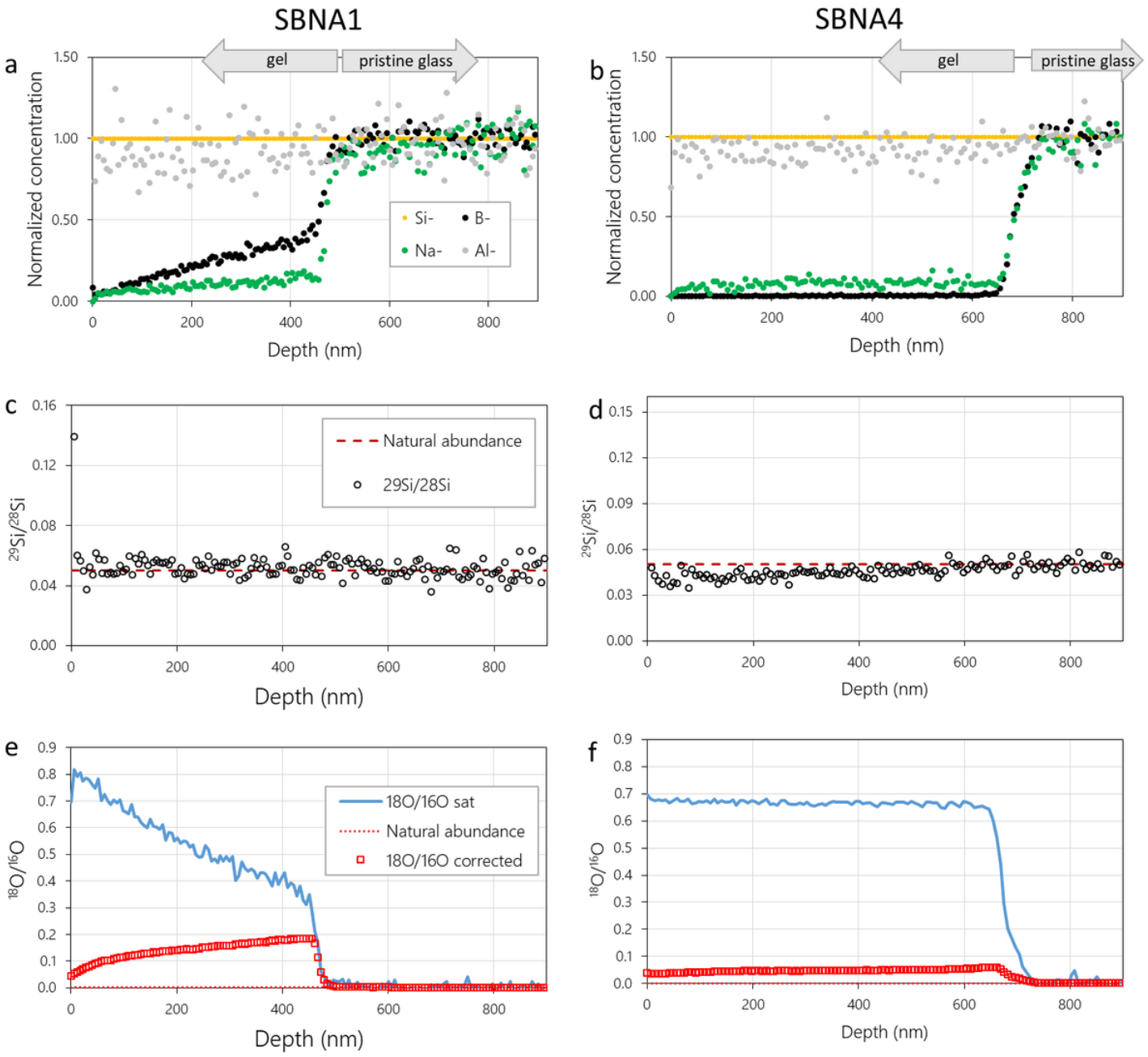

Figure 6

ToF-SIMS analysis of SBNA1 and SBNA4 glass altered coupon. Alteration ran for 1 month in a Si saturated solution at 90°C, followed by 1 day in $H_2{}^{18}O$ at room temperature. **a** and **b**, B, Na, and Al profiles recorded in negative mode and normalized to Si. **c** and **d**, $^{29}Si/^{28}Si$ profiles compared to natural abundance (0.05) indicated in dotted line. **e** and **f**, $^{18}O/^{16}O$ profiles (red) compared to that expected if the porosity left by the release of B and Na is saturated with ^{18}O labelled water. $^{18}O/^{16}O$ at natural abundance (0.002) is indicated in dotted line. This is the value obtained in the pristine glass.